

Numerical experiments on the movement of a warm-core ring with the bottom slope of a western boundary

S. Itoh and T. Sugimoto

Division of Fisheries Environmental Oceanography, Ocean Research Institute, University of Tokyo
Tokyo, Japan

Abstract. Numerical experiments are performed to investigate the effects of the bottom slope of a western boundary on realistic warm-core rings, using a primitive equation sigma coordinate model. Warm-core rings which initially have baroclinic velocity near a steep bottom slope gradually move northward, but those with barotropic velocity do not. Barotropic velocity on the slope immediately disperses as a topographic Rossby wave, while baroclinic velocity is retained. Since the northward movement is caused by an effect very much like the image effect which is originally the effect of a free-slip wall, the authors term this effect the equivalent image effect. The equivalent image effect increases as a slope becomes steeper and bottom friction becomes weaker, and vice versa. It seems that a steep slope acts like a wall, and the bottom friction of a steep slope corresponds to the lateral viscous effect of a wall. However, the effect of a slope on a warm-core ring is different from that of a wall in that ring-slope interactions take place at the lower part of the ring. Because the velocity of a warm-core ring is weak in deep layers, ring-slope interactions are moderate and the leakage of the interior fluid of a ring seen in ring-wall interactions is not apparent, while the viscous effect is weaker than that of a no-slip wall as well. These results are applied to the northward movement of Kuroshio warm-core rings and to warm eddies in the Gulf of Mexico.

1. Introduction

Intense warm-core rings often detach from the Kuroshio Extension and remain for several years in the Kuroshio-Oyashio transition zone. These are large baroclinic anticyclones whose radii are ~ 100 km and maximum velocities exceed 1 m s^{-1} . Warm-core rings in the Kuroshio-Oyashio transition zone tend to move to the north along an isobath of ~ 3000 – 6000 m [Hata, 1974; Yasuda *et al.*, 1992] even though there is no corresponding large-scale northward current. For example, in the spring of 1993, warm-core ring 93A, which detached from the Kuroshio Extension, was initially located at $37^{\circ}30'N$ but by December 1997 it reached $42^{\circ}N$ (Figure 1). Many observed warm-core rings are also distributed along the Japan trench, extending to the north (Figure 1). This is one of the characteristic features of Kuroshio warm-core rings compared to similar eddies observed near other western boundary regions, where few eddies migrate poleward for such long distances. Gulf Stream warm-core rings, for example, tend to move southwestward along an isobath of 2000 – 3000 m [Brown *et al.*, 1986].

Recently, Yasuda [1995] suggested that the northward motion of Kuroshio warm-core rings is heton-type of vortex propagation [Hogg and Stommel, 1985]. However, this theory is not enough to explain the seasonal north-south oscillation and the long-term northward movement of warm-core ring 93A. The northward alongshore movement suggests that the topographic nonlinear effect [Cox, 1979] is dominant compared to other effects such as the nonlinear planetary β effect, which drives an anticyclone to the southwest [McWilliams and Flierl, 1979].

Copyright 2001 by the American Geophysical Union.

Paper number 2001JC000789.
0148-0227/01/2001JC000789\$09.00

Under the planetary β effect, the western (eastern) half of a warm-core ring which has northward (southward) velocity exhibits a negative (positive) planetary vorticity advection. This results in a westward shift of the vorticity center, and if nonlinearity is strong enough, it is associated with the generation of a secondary anticyclone and cyclone on the western and eastern flanks of the warm-core ring, respectively. This vorticity shift and the advection of the two secondary vortices drive the warm-core ring southwestward. There is also a linear southward force called the β force. This force is exerted by the imbalance of northward and southward Coriolis forces. In an open ocean this force balances with the northward Coriolis force due to the westward movement of a ring [Nof, 1981] and does not cause the meridional motion. However, as a ring approaches a western boundary and the westward motion decelerates, the importance of the β force increases. The topographic nonlinear effect stated by Cox [1979] is generally called the image effect [Sommerfeld, 1950]. In two-dimensional nondivergent theory, an anticyclonic vortex line near a western wall moves to the north owing to a side boundary effect, and this is equivalent to that of a mirror cyclone opposite to the wall. An anticyclone near a free-slip western wall can move northward even under the planetary β effect [Yasuda *et al.*, 1986; Shi and Nof, 1994].

However, there are several difficulties in applying the image effect to the real ocean. This is not due to the slope but to a free-slip wall, and specifically, it is based on the invertibility principle [Hoskins *et al.*, 1985]. The invertibility principle in geophysical fluid dynamics implies that all the variables of the field should be uniquely determined by the potential vorticity distribution and the given boundary conditions. The quasi-geostrophic equations are invertible, but the primitive equations are not [Sansón *et al.*, 1998]. Even if the image effect is valid for a slope, it is not the only driving force caused by the

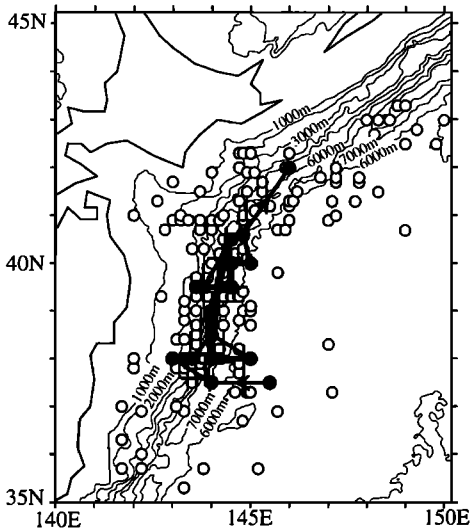


Figure 1. Observed positions of warm-core rings. Open circles show the distribution of warm-core rings observed from 1957 to 1973 (adapted from Kitano [1975]). The trajectory of warm-core ring 93A is shown with solid circles and lines.

bottom topography. The topographic β effect of a western boundary slope drives an anticyclone to the southeast [Smith, 1986], while among wall effects the rocket effect [Shi and Nof, 1994] is also important. Thus, how a real western boundary acts on warm-core rings is complex.

Most examinations of the mechanisms of a warm-core ring's behavior were studied through numerical experiments. Some previous studies adopted two-layer models with a bottom slope [Smith and O'Brien, 1983; Smith, 1986; Matsuura and Kamachi, 1989; Thierry and Morel, 1999; Sansón and van Heijst, 2000], but this is not enough to examine the topographic effects in detail. The near-bottom velocity of a warm-core ring causes the topographic β effect, but velocity is uniform from the main thermocline to the bottom in most two-layer models, and the topographic β effect was often overestimated. In this study we use a numerical model with fine vertical resolution instead, and we examine the effect of the bottom slope of a western boundary on warm-core rings. Because the steep bottom slope of the Japan trench may act like a free-slip wall on Kuroshio warm-core rings, we especially focus our interest on whether or not a steep slope behaves like a wall. We first examine the behavior of several warm-core rings, each of which has a different structure, and we then vary slope and bottom friction. By using these variables, we can compare a slope with both a free-slip and a no-slip wall. Finally, we discuss the application of these experiments to the dynamics of warm-core rings in the Kuroshio-Oyashio transition zone.

In section 2 we provide a brief introduction to the numerical model and its boundary conditions, describe the initial condition, and explain each experiment in detail. These results are presented in section 3. In section 4 we analyze the results and discuss their applications. We conclude the study with a summary in section 5.

2. Method

2.1. Numerical Model

We adopt a model based on the Princeton Ocean Model (POM) [Mellor, 1998]. POM is a three-dimensional, primitive

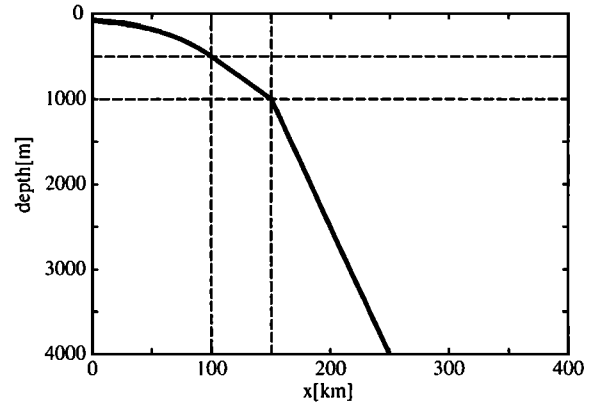


Figure 2. East-west section of the bottom topography near a western boundary region in the case where $\delta h_x = 30$.

equation, sigma coordinate model and is suitable to our objective of investigating slope effects.

The basic equations consist of the continuity equation, the horizontal momentum equations, the energy (temperature) equation, and the equation of state. We fixed salinity, vertical diffusivity, and viscosity as constants with values of 34 psu, $10^{-4} \text{ m}^2 \text{ s}^{-1}$, and $10^{-4} \text{ m}^2 \text{ s}^{-1}$, respectively. By doing so, we are able to simplify our model by eliminating the salinity equation and the turbulent closure submodel equations. We also consider the horizontal diffusivity and viscosity as constants instead of using Smagorinsky diffusivity in POM. Although it is easy to calculate, we select using constants for both of the vertical and horizontal coefficients for simplicity. These values are set at $100 \text{ m}^2 \text{ s}^{-1}$.

The model domain is $1200 \text{ km} \times 1200 \text{ km}$ with bottom topography. The Coriolis parameter used is that corresponding to each latitude between 32°N – 43°N . The slope of a western boundary is set as the bottom topography in the form.

$H =$

$$\begin{cases} 67.668 \exp(0.02X) & (0 \leq X < 100), \\ 500 + 10(X - 100) & (100 \leq X < 150), \\ 1000 + \delta h_x(X - 150) & (150 \leq X < 150 + 3000/\delta h_x), \\ 4000 & (150 + 3000/\delta h_x \leq X \leq 1200), \end{cases} \quad (1)$$

where H is the depth (m), X is the distance from the western boundary (km), and δh_x is the slope (m km^{-1}). The slope of the real western boundary region is about $h_x = 50 \text{ m km}^{-1}$ at the Kuroshio-Oyashio transition zone and off the east Australian coast, while $h_x = 10 - 20 \text{ m km}^{-1}$ at the Gulf Stream region and the Gulf of Mexico. Figure 2 shows an east-west cross section of the bottom topography (see also Figure 11). Horizontal grid spacing is 10 and 5 km in the meridional and zonal direction, respectively. High zonal resolution is used in order to avoid the computational error caused by a steep slope [Mellor et al., 1994]. The sigma grid spacing is finer in the upper part of the water columns but also uses moderate spacing in the lower part to resolve the deep structure of warm-core rings (Table 1). No external forcing, such as wind stress, solar radiations, and mass fluxes, is considered, but we permit the transmission of noisy waves at the side boundaries. Drag force $\vec{\tau}$ due to bottom friction is described in the equation

Table 1. Sigma Levels in the Model

Level	Value
1	0.00
2	-0.010
3	-0.020
4	-0.030
5	-0.040
6	-0.052
7	-0.064
8	-0.081
9	-0.101
10	-0.126
11	-0.157
12	-0.197
13	-0.246
14	-0.307
15	-0.384
16	-0.480
17	-0.600
18	-0.700
19	-0.800
20	-0.900
21	-1.000

$$\vec{\tau} = \rho C_z |\mathbf{v}|^2 \mathbf{v}, \quad (2)$$

where C_z is the drag coefficient and

$$C_z = C_0 \times \max \left(\frac{k^2}{[\ln(\Delta\sigma_b H/z_0)]^2}, 0.0025 \right), \quad (3)$$

where $k = 0.4$ is the von Karman constant, $z_0 = 0.01$ m is the roughness parameter, $\Delta\sigma_b = 0.1$ is the bottom sigma grid spacing, and H (m) is the in situ depth. In our experiments the left term in the bracket is smaller than 0.0025 for the region deeper than 300-m depth. C_0 is a constant through which we can control bottom friction.

2.2. Initial Structure of Warm-Core Rings

All experiments are initialized with axisymmetric warm-core rings in a motionless ocean and then run for a 200-day simulation. Details in the ring structure must be stated deliberately

since they appear to be critical in the investigation of bottom slope effects. Unlike two-layer models, we can reproduce a realistic structure of a warm-core ring not only horizontally but also vertically. We at once assume the potential temperature field θ as follows:

$$\theta = \bar{\theta} + \theta', \quad (4)$$

$$\bar{\theta} = 15 + \frac{25}{\pi} \tan^{-1} \left(\frac{z}{167} \right), \quad (5)$$

$$\theta' = \Delta\theta_{\max} \times \exp \left(\frac{1}{2} \right) \times \frac{2z}{h_0} \exp \left(-\frac{z^2}{2h_0^2} - \frac{r^2}{r_0^2} \right), \quad (6)$$

where $\bar{\theta}$ and θ' denote a basic field and an anomaly, r_0 , h_0 , and $\Delta\theta_{\max}$ are specific radius, thickness, and maximum potential temperature anomaly of a warm-core ring, respectively. For the basic field, temperature ranges from 15°C at the surface to 2.5°C in the deepest layer, the thermocline depth being ~500 m. Although some previous studies assumed geostrophy, the velocity structures of warm-core rings in the real ocean are not clear. Some warm-core rings at the Kuroshio-Oyashio transition zone were observed to be gradient current rather than geostrophic [Itoh, 1999]. We adopted the gradient current approximation and calculated baroclinic velocity. However, the estimated potential temperature based on observed density cannot reproduce the velocity profiles of intense warm-core rings. Kawasaki *et al.* [1990] detected a warm-core ring velocity of ~0.1 m s⁻¹ at 1885-m depth with a current meter, but in our study, the calculated baroclinic velocity using estimated r_0 , h_0 , and $\Delta\theta_{\max}$ from observations practically vanishes below 1500-m depth (Figure 3a). The calculated maximum velocity is also smaller than that observed by acoustic Doppler current profiler (ADCP); it is at most 1.2 m s⁻¹, though observed velocity by ADCP often exceeds 1.5 m s⁻¹ [Itoh, 1999]. These underestimations are probably caused by either (1) a barotropic component or (2) an inadequate potential temperature (equivalent to density in our model) structure, or perhaps both. We consider both of these possibilities. The barotropic velocity is simply added to the baroclinic velocity and calculated as

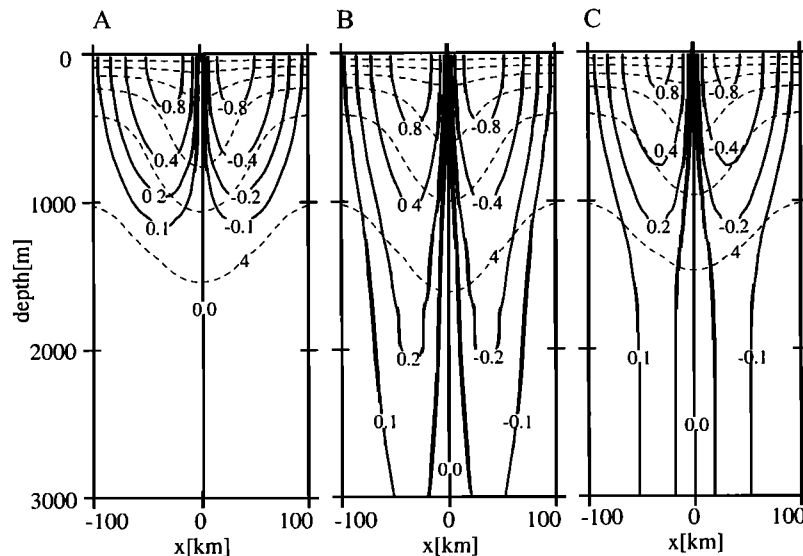


Figure 3. Initial velocity and temperature sections of cases (a) C, (b) D, and (c) A. Structural parameters are listed in Table 2.

Table 2. Parameters of Experiments^a

Case	Structure	δh_x	C_0
A	$\Delta\theta_{\max} = 3, \Delta\theta'_{\max} = 0.3, h' = 2000, \alpha = 0.0$	30	1.0
B	$\Delta\theta_{\max} = 3, \Delta\theta'_{\max} = 0.6, h' = 1000, \alpha = 0.0$	30	1.0
C	$\Delta\theta_{\max} = 3, \Delta\theta'_{\max} = 0.0, \alpha \pm 0.2$	30	1.0
D	$\Delta\theta_{\max} = 4, \Delta\theta'_{\max} = 0.0, \alpha = 0.0$	30	1.0
E	same as case A	40	1.0
F	same as case A	20	1.0
G	same as case A	30	10
H	same as case A	30	0.1

^aIn all cases, $r = 50$ km, $r' = 50$ km, and $h = 500$ m.

$$V_{bt} = \alpha V_{bc}, \quad (7)$$

where α is a constant and V_{bc} is the surface baroclinic velocity referenced at an infinite depth. Figure 3b shows an example modified by the barotropic velocity. The modification of the potential temperature structure is done by adding another baroclinic ring whose temperature anomaly is smaller, but extends deeper, than the original one. For this ring the notations of $r'_0, h'_0,$ and $\Delta\theta'_{\max}$ are used. Even though $\Delta\theta'_{\max}$ is very small, moderate magnitude of supplementary velocity can be obtained only if h'_0 is large enough. A small $\Delta\theta'_{\max}$ and large h'_0 modify the velocity profile but hardly change the density profile (Figure 3c).

We now have seven parameters: $r_0, h_0, \Delta\theta_{\max}, r'_0, h'_0, \Delta\theta'_{\max},$ and α for the ring structure. Parameters $r_0, h_0,$ and $\Delta\theta_{\max}$ are estimated from observations: $r_0 = 40 \sim 70$ km, $h_0 = 300 \sim 500$ m, and $\Delta\theta_{\max} = 2 \sim 4^\circ\text{C}$. However, $r'_0, h'_0, \Delta\theta'_{\max},$ and α cannot be done in the same way. We set $r'_0 = r_0$ in all the experiments and use either h'_0 and $\Delta\theta'_{\max}$ or α for the modification. Parameters h'_0 and $\Delta\theta'_{\max}$ or parameter α is determined so that there should be a moderate velocity consistent with observations in deep layers, although direct observations are rare.

2.3. Cases

In Table 2 we list our experiments. Cases A–D are for examining the behavior of warm-core rings, each of which have a different structure. In cases A and B, rings have deep baroclinic structure, while the ring in case C has barotropic velocity and that in case D has no velocity in the deep layer. Note that the ring in case A has a deeper structure than that in case B. We select case A as the reference case and analyze the effects of the gradient of a slope and bottom friction in cases E and F and cases G and H, respectively.

3. Results

3.1. Flat Bottom Cases

Before performing experiments with a western boundary slope, we model those with a flat bottom and a vertical western wall. A warm-core ring far from the wall moves to the southwest owing to the nonlinear planetary β effect, as in the work of *McWilliams and Flierl* [1979]. On the other hand, those near a wall are greatly influenced by it, and the effects depend on the side boundary condition: free-slip or no-slip. A ring near a free-slip wall moves northward, but that near a no-slip wall moves slightly to the south as in the work of *Yasuda et al.* [1986]. Because the ring in a free-slip experiment is strongly deformed to be semicircular and leaks the interior fluid southward, the mechanisms of the northward movement are sug-

gested to be the combined effects of the image effect and the rocket effect as discussed by *Shi and Nof* [1994]. That in a no-slip wall experiment does not approach the wall so much as the free-slip one, and those effects are not strongly apparent. The offshore tendency is due to the advection of a cyclonic eddy on the northern flank generated by the friction, which was seen in the experiments of ring-wall (stated as “vortex-wall” in their study) interaction [*Sansón et al.*, 1999].

In cases with a slope we initially place rings at the edge of the slope region. Sections 3.2–3.4 present the results of experiments with a slope changing the deep structure of rings, the gradient of the slope, and bottom friction.

3.2. Effect of the Deep Structure of Rings

First, we carry out the experiments for investigating various deep structures of warm-core rings. In section 2.2, $r_0, h_0,$ and $\Delta\theta_{\max}$ are estimated on the basis of observations, but $r'_0, h'_0, \Delta\theta'_{\max},$ and α still remain ambiguous. Four cases of A–D (Table 2) are examined. Figure 4 presents the surface velocity vector distribution of these four cases at days 0, 50, 100, 150, and 200. The approximate location of the ring in case A is also shown by a large circle so comparisons can be made between each case. There are distinct differences in meridional movement, though gradual westward movement is common in all cases. After 200 days calculation the warm-core ring in cases A, B, C, and D moves to (–60 km, 185 km), (–60 km, 80 km), (–60 km, 100 km), and (–60 km, 30 km), respectively. Taking into account the initial structure of the rings (Table 2), it is inferred that deep baroclinic velocity interacts with the bottom topography and drives warm-core rings to the north.

Figure 5 shows the velocity vector distribution and the potential temperature contours at 1750-m depth at day 100. The warm-core rings in cases A and B retain anticyclonic velocity, and secondary cyclones due to the nonlinear planetary β effect develop to the southeast of the rings. The semicircularly deformed velocity profiles of warm-core rings suggest the appearances of an effect equivalent to the image effect, because a circular anticyclone advected by a mirror cyclone would form such a shape. Hereinafter, we call this effect the equivalent image effect, and a more detailed discussion of this effect takes place in section 4.1. Unlike a ring-wall interaction, southward leakage of the interior fluid is very little, and the rocket effect must be weak. This is because the rings interact with a slope mainly in deep layers where velocity is relatively weak. Hence the northward movement in cases A and B is due to the equivalent image effect. This consideration also matches the marked northward moving tendency of the warm-core ring in case A compared to case B, since the near-bottom velocity of the ring is stronger in case A. For the rings in cases C and D, however, anticyclonic velocity is not present, and the devel-

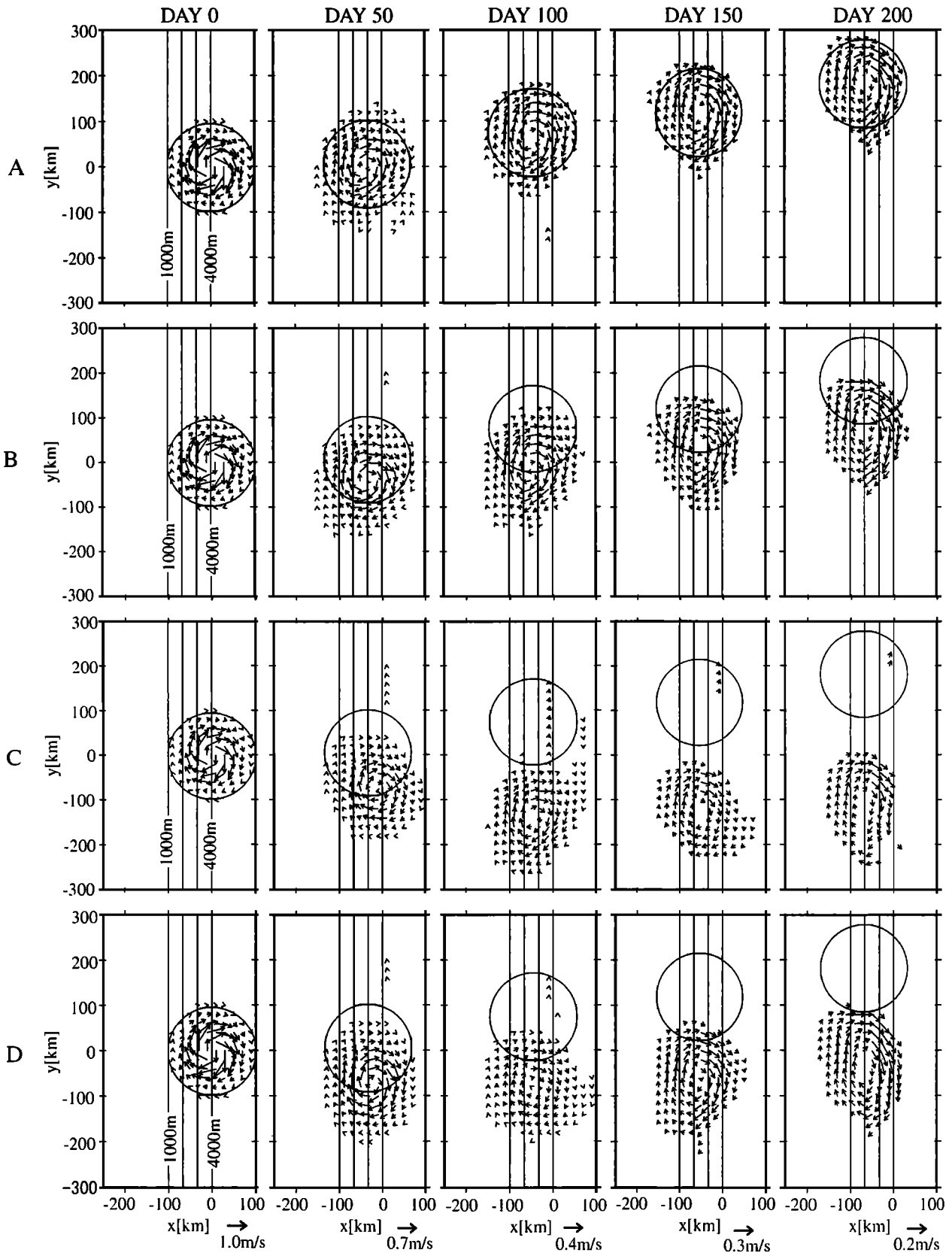


Figure 4. (a–d) Surface velocity profiles of cases A, B, C, and D at days 0, 50, 100, 150, and 200. The x and y coordinates are set so that the initial location of the warm-core rings was at $x = 0, y = 0$. The large circles indicate the position of the warm-core ring in case A.

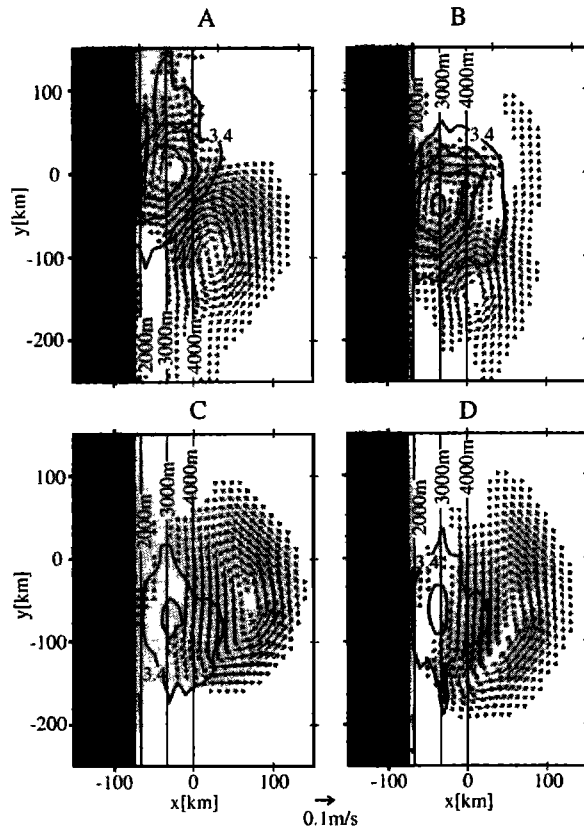


Figure 5. The 1750-m depth velocity (vectors) and temperature (solid lines) profiles of cases (a) A, (b) B, (c) C, and (d) D at day 100. Temperature contour interval is 0.1°C . Shaded region is land.

oped cyclones at the east advect the rings southward. It also seems that the northward movement of a ring decreases the influence of the southward advection of the cyclone because its relative location to the ring shifts southwestward.

The ring in case C initially has a barotropic velocity (Table 2), but by day 100 (Figure 5) it vanishes completely. It disperses as a topographic Rossby wave, because the barotropic velocity on a slope is directly affected by the topographic β effect. This is the same phenomenon presented in the previous two-layer experiment by *Thierry and Morel* [1999]. The topographic beta parameter β_T at the 2000–4000 m depth in our model is $\sim 1 \sim 2 \times 10^{-9} \text{ m}^{-1} \text{ s}^{-1}$, much larger than the planetary beta parameter of $2 \times 10^{-11} \text{ m}^{-1} \text{ s}^{-1}$. Baroclinicity can reduce this dispersion with the joint effect of baroclinicity and bottom relief (JEBAR) effect [*Mertz and Wright*, 1992], and this is the reason for the maintenance of deep velocity in case A.

Among the four cases the case A warm-core ring shows a movement pattern similar to the long-term movement of Kuroshio warm-core rings. Therefore we adopt the same structure used in case A for the following experiments.

3.3. Effect of the Gradient of a Slope

Next, we perform the experiments by changing the gradient of the slope. The initial location of each warm-core ring is at the edge of the slope region. Figure 6 shows the surface velocity vector distribution of cases E and F. The ring in case E moves northwestward at day 0–50 while that in case A moves westward, but at day 50–200 both of the rings move at a similar

northward velocity. At day 200 those of cases A and E reach the location (–60 km, 185 km) and (–50 km, 195 km), respectively. The case F ring moves southwestward at day 0–50 and gradually turns its direction to northwestward at day 50–100. At day 100–200 it still keeps a westward tendency, and the northward speed is small compared to those in cases A and E. The final location of the ring in case F is (–90 km, 10 km). The differences of the movement of these rings are summarized to the following two points. For the first, there is the difference in day 0–50: The rings in cases A, E, and F move westward, northwestward, and southwestward, respectively. For the second, at day 50–200 the movement of the case F ring is different from those in cases A and E, which show a similar tendency in this term. Considering the setting of these three experiments, there is a difference between these two points in the way a ring interacts with a slope.

As seen in Figure 6, the rings in these three cases always move westward owing to the planetary β effect, although their speed is variable. This is a very important factor for the interaction between warm-core rings and the bottom slope of a western boundary; rings detached from a western boundary current inevitably encounter the bottom topography of a western boundary. In our experiment the temporal location is referred to the initial location, and this initial location is set to the edge of the slope region. Accordingly, a coastal location follows a steep slope. Ring-slope interactions take place initially at the edge of the slope region for all three rings, but as the rings intrude the slope region, how they interact with a slope depends on to what extent they go up the slope. The distance of the rings from the coast at day 50 for cases A, E, and F is, for example, 205, 215, and 260 km, respectively, and accounts for the second point in part; despite the largest westward move of the three, the ring in case F is still far from the boundary. This resembles the initial position problem in the work of *Sansón et al.* [1999], who presented the dependence of the movement on the initial position from a wall, whereas things are not so simple in our experiments with a slope because a ring-slope interaction is always active in the lower part of a ring. Further analysis is needed for this interaction near a bottom.

Figure 7 shows the velocity vector distribution and the potential temperature contours at 1750-m depth corresponding to cases E, A, and F at day 5. We find that the steeper the slope is, the more the rings are deformed in a semicircular fashion, which is the appearance of the equivalent image effect. Southward flow at the south of the rings also increases with the gradient of a slope yet is not so strong as to leak the core water of the rings as seen in the potential temperature profile. Therefore a steep slope directly causes the equivalent image effect to be strong, and the westward movement of the rings increases this tendency.

3.4. Effect of Bottom Friction

We now discuss the results for different values of C_0 , which is fixed as 1.0 in all of the preceding experiments. We set $C_0 = 10.0$ in case G and $C_0 = 0.1$ in case H. Figure 8 shows the surface velocity vector distribution of these two cases. Despite the difference in friction, there are no clear dissipative effects, except for disturbances seen in the shallow region. Disturbances propagating westward usually vanish in a western shallow region where bottom friction is relatively large, but weak friction cannot completely dissipate them (case H in Figure 8).

There is an apparent quantitative difference in movement

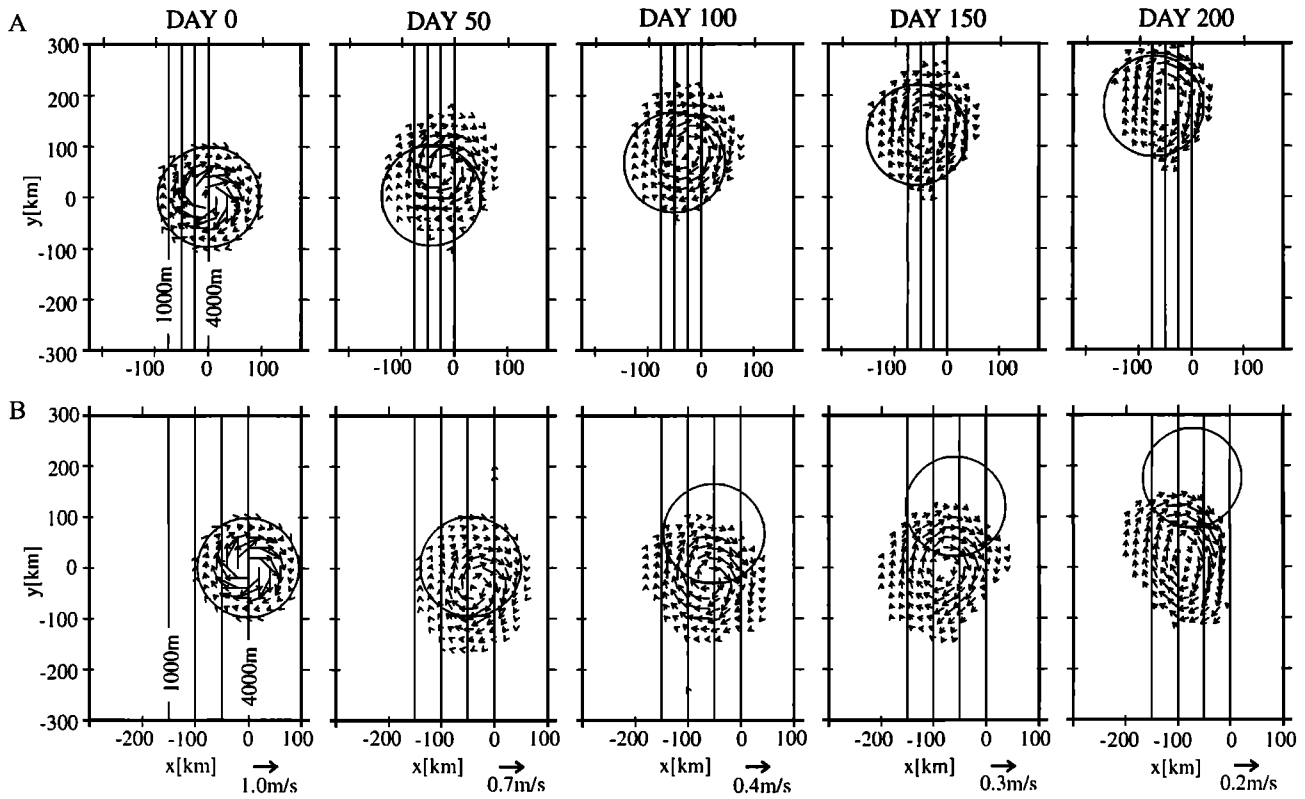


Figure 6. Same as Figure 4 but for cases (a) E and (b) F.

rather than dissipation. At day 200 the ring in cases A, G, and H are at $(-60 \text{ km}, 185 \text{ km})$, $(-50 \text{ km}, 325 \text{ km})$, and $(-75 \text{ km}, 30 \text{ km})$, respectively. The northward movement dramatically increases (decreases) with the decrease (increase) of bottom friction, while the westward movement slightly tends to do so. This result can be related to the previous experiments of a ring-wall interaction in which a no-slip wall prevents the rings from moving northward through a cyclone generated on the northern flank. However, the cyclone does not clearly appear here in the experiments with a slope, and a ring moves northward even if friction is large (Figure 8b). This is again accounted for by the moderateness of a ring-slope interaction,

since velocity near the bottom is by far the weaker than that near the surface.

4. Discussion

4.1. The Equivalent Image Effect

From a theoretical point of view, the application of the image effect to the real ocean has many difficulties as mentioned in section 1. However, an effect very much like the image effect appears in the deep layer in our realistic numerical experiments. Warm-core rings are semicircularly deformed near the bottom slope of a western boundary and move north-

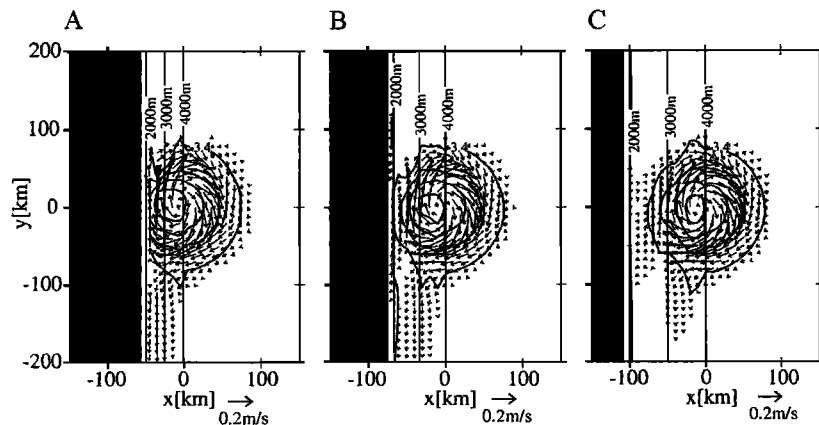


Figure 7. Same as Figure 5 but for cases (a) E, (b) A, and (c) F at DAY 5.

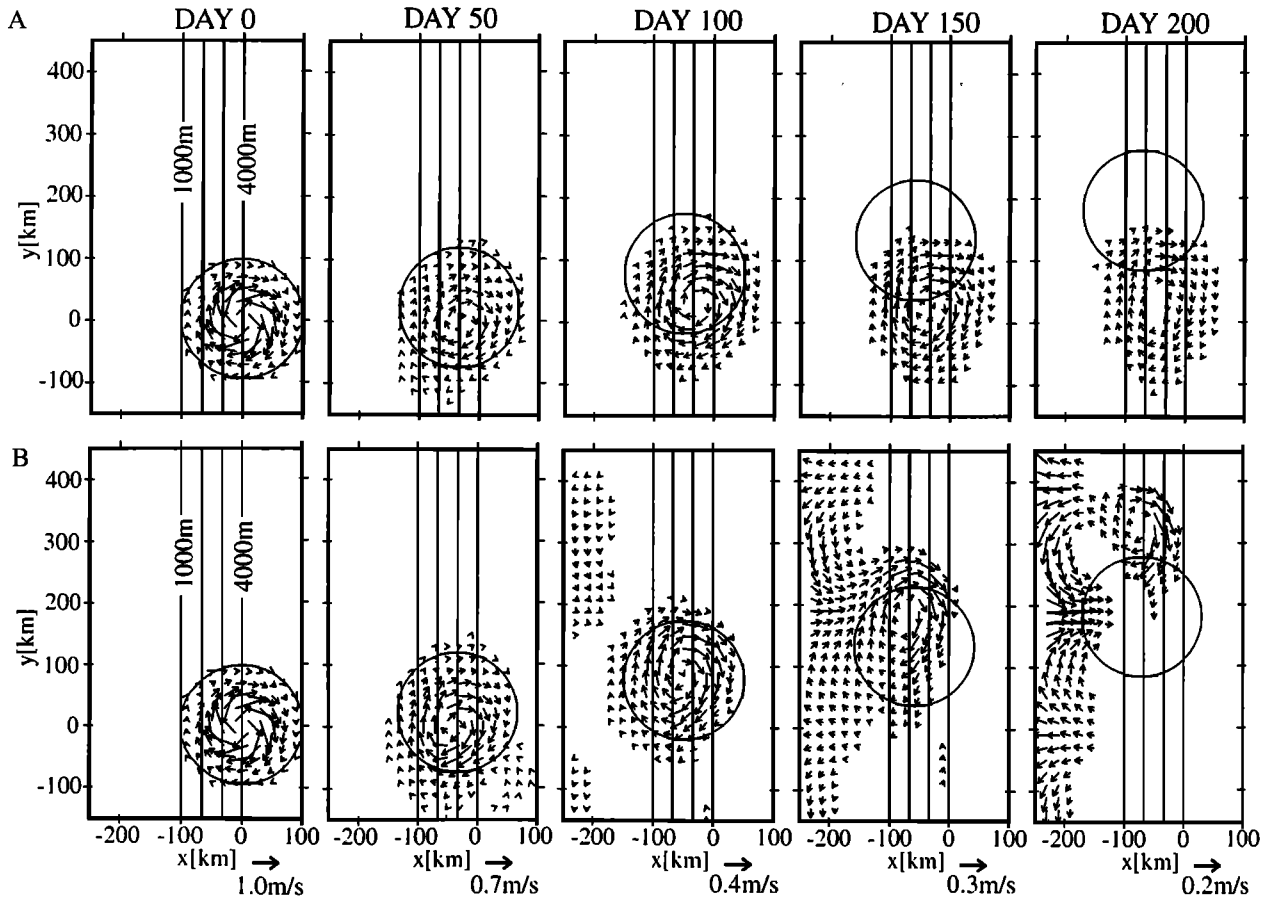


Figure 8. Same as Figure 4 but for cases (a) G and (b) H.

ward. We consider the semicircular deformation as an indication of an effect equivalent to the image effect. Now we examine this equivalency by decomposing a semicircular velocity field into a vortex pair, and we discuss its behavior.

Suppose the velocity profiles of an original eddy and a decomposed eddy are $(u(x), v(x))$ and $(u'(x), v'(x))$ for an east-west section, respectively. For the decomposed eddy we require zonal symmetry along $x = a$. The relationship between the velocities of the original eddy and the decomposed eddy is

$$u(x) = u'(x) - u'(-x), \tag{8a}$$

$$v(x) = v'(x) - v'(-x). \tag{8b}$$

The second term on the right of the equations is the mirror velocity component. Using the zonal symmetry, this is rewritten as

$$u(x) = u'(x) - u'(2a + x), \tag{9a}$$

$$v(x) = v'(x) + v'(2a + x). \tag{9b}$$

For an eddy that is nearly symmetric in the north-south direction, we can consider a as a constant. With these assumptions we can convert eddies into vortex pairs using the least squares method. Figure 9 shows the 1750-m depth velocity from case F at day 5 and a decomposed vortex pair. Since the coefficient of determination is $R^2 = 0.92$, decomposition is nearly complete. Now the problem is whether the vortex pair can move steadily northward or not. The pair of vortex lines in two-

dimensional nondivergent theory could do so, but our realistic experiments are nonlinear, and the potential vorticity distribution is very complex. However, in the analogy of the interaction between two like-signed vortices [Yasuda, 1995], we expect that they would gradually advect each other, undergoing streamer development. Although the upper part of an eddy is not directly influenced by topography, it is tightly coupled to the lower part through hydrostatic balance. All things considered, a steep slope deforms a warm-core ring into a semicircle, and this deformation induces northward movement associated with other slight deformations or partial splitting.

4.2. Mechanism of the Movement of Warm-Core Rings

The validity of the equivalent image effect is demonstrated in the preceding discussion. It suggests that it is dominant for the northward movement of the rings, because there appear semicircular deformation and the little leakage on the rings moving northward. We examine this implication and then discuss the general mechanism of the warm-core rings movement near a bottom slope.

As stated before, there are other important effects for the meridional movement of the rings near the bottom slope of a western boundary. These are the β force, the nonlinear β effect, the topographic β effect, and the rocket effect. The former three effects drive warm-core rings southward, and the last drives warm-core rings northward. The significance of the equivalent image effect and the nonlinear planetary β effect is presented in cases A–D (Figure 5) and that of the other three

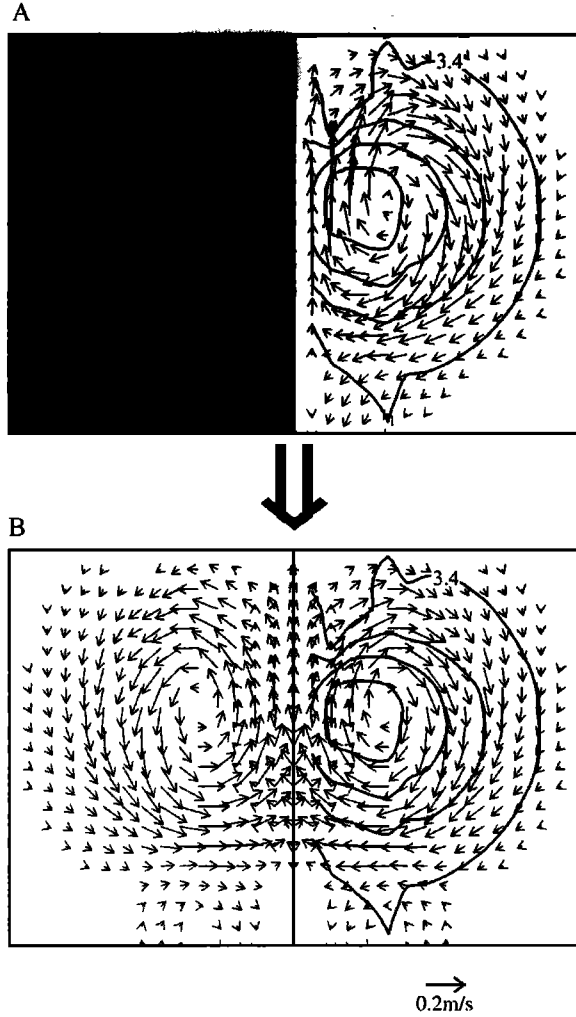


Figure 9. Example of the decomposition of a warm-core ring into a vortex pair: (a) 1750-m depth velocity profile of case F at day 5 and (b) a decomposed vortex pair through the least squares method. The coefficient of determination is $R^2 = 0.92$. Although the left half of Figure 9a represents land, a virtual mirror image of the eddy is displayed in Figure 9b.

effects is shown in the order estimation of the previous studies [Shi and Nof, 1994; Nof, 1999; Sansón and van Heijst, 2000]. Shi and Nof [1994] and Nof [1999] suggested that the β force and the rocket effect are the major effects for the meridional movement for a intense warm-core ring near a western boundary. Sansón and van Heijst [2000] showed the importance of the topographic β effect for the movement of barotropic vortices, but the topographic β effect is rather strong for a western boundary slope, and as seen in case C, the velocity on the slope immediately disperses away [Thierry and Morel, 1999].

The β force is presented to be the only meridional force for the center of mass of a ring which has stopped its westward migration by a western wall [Sansón et al., 1998; Nof, 1999]. It appeared in the integral expression of the momentum equations [Nof, 1981; Killworth, 1983; Cushman-Roisin et al., 1990; Sansón et al., 1998]. Sansón et al. [1998], for example, defined the coordinate of a ring's center of mass as

$$X = \frac{1}{V} \int x h dx dy, \quad (10)$$

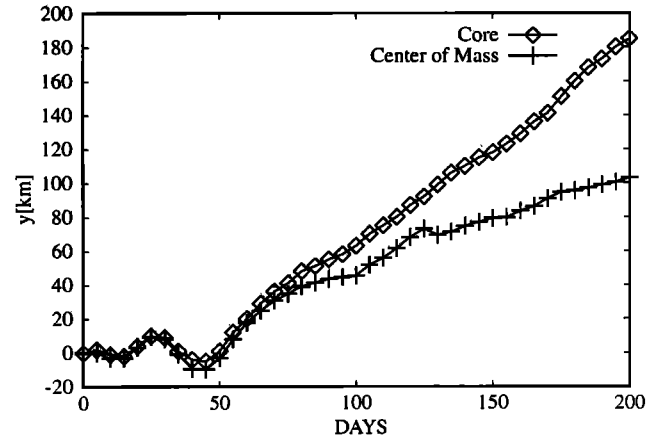


Figure 10. Meridional location of the core of the ring (diamonds) and the center of mass (crosses) in case A. The water whose potential temperature is higher than that of the basic field by 0.1°C are considered to be originated from the rings, and weighted averages are taken for the region $-1000 \text{ km} < y < 1000 \text{ km}$, $-200 \text{ km} < x < 200 \text{ km}$.

$$Y = \frac{1}{V} \int y h dx dy, \quad (11)$$

where h is the thickness anomaly of a ring and

$$V = \int h dx dy = \text{const.} \quad (12)$$

They differentiated these coordinates, put them into the integrated momentum equations weighted by h , and got the momentum equations for the ring's center of mass. Expressing the β force as F_β and a zonal force due to a meridional western wall as F_x , these are rewritten in a dimensional form as

$$\frac{d^2X}{dt^2} - f \frac{dY}{dt} = F_x, \quad (13)$$

$$\frac{d^2Y}{dt^2} + f \frac{dX}{dt} = F_\beta. \quad (14)$$

If the term dX/dt vanishes, the ring accelerated southward. F_x is generally eastward (positive), and the southward velocity is equal to $-F_x/f$ (negative). However, some of the rings in our experiment move northward. According to the above formulation, this must be because of mass leakage toward the south: the rocket effect. Although little leakage is seen in the result, we should reexamine the rocket effect. Figure 10 shows the meridional positions of the warm core and the mass center of the warm-core ring water in case A. The center of mass approximately coincides with the position of the warm core until day 60, and then it gradually drops behind the warm core but still moves northward to reach the 100 km north at day 200. Actually, this meridional distance of the center of mass might be underestimated as we cannot completely distinguish ring's water from disturbances, but it is certain that the center of mass moves northward. This implies that there is another meridional force.

The reason that the β force was presented to be the single meridional force is because we ignore the term

$$\int x \frac{dh}{dt} dx dy, \int y \frac{dh}{dt} dx dy$$

in the expressions of the dX/dt and dY/dt . Ball [1963] stated that this term becomes nil by proper interpretation of $dx dy$, yet these terms are generally not zero if an integration take place for a specific area. Since $dh/dt = h(\partial u/\partial x + \partial v/\partial y)$, these terms are responsible for adjustment processes for nearly gradient current [Itoh, 1999] warm-core rings. Detail formulation is complex and beyond our scope, but it is said that the image effect accompanies the adjustment because it does not advect mass but relative vorticity along a wall. The northward movement of a ring shows that the β force is not dominant to other northward forces.

Now the direct effects to be considered for the meridional movement of a ring are the equivalent image effect and the nonlinear β effect, and these are estimated in the dimension of velocity. In a nonrotating frame of reference the velocity of a vortex line V_i along a wall due to the image effect V_e is written as

$$V_i = \frac{\Gamma}{4\pi l}, \quad (15)$$

where Γ is the circulation of the vortex and l is the distance from the vortex center to a wall. Then the velocity of the equivalent image effect can be roughly estimated using this formulation. Proper $\Gamma(z)$ and $l(z)$ give the velocity of the equivalent image effect as

$$V_e = \alpha \frac{\int \{\Gamma(z)^2/l(z)\} dz}{4\pi \int \Gamma(z) dz}. \quad (16)$$

The coefficient α is multiplied because the image effect transports relative vorticity. We consider $\alpha = 0.5$, which implies that the horizontal scale of a ring is the same as the internal radius of deformation. Assuming the vertically averaged values of the ring's radius, distance to a coast, and angular velocity to be 100 km, 50 km, and $0.01 f$, respectively, $V_e \sim 2.5 \text{ cm s}^{-1}$. The southward advection due to the nonlinear β effect is estimated by the intensity of the secondary vortex pair formed on the eastern and western flanks of a ring. If we assume adjustment time to be $O(f)$, the intensity is $O(\beta v/f)$, and the velocity induced by these vortices is $O(\beta vL/f)$, where L is the horizontal scale of a ring. The values of $v \sim 1 \text{ m s}^{-1}$ and $L \sim 100 \text{ km}$ give the induced southward velocity to be $V_n \sim 2 \text{ cm s}^{-1}$. This is the same order as V_e and the southward migration speed of a warm-core ring in an open ocean.

The equivalent image effect and the nonlinear β effect are proved to be the two major comparable effects in our experiments. The equivalent image effect increases for increasing nonlinearity and decreasing average distance to a boundary, while the nonlinear β effect depends only on nonlinearity. Hence, comparing the average distance is useful in understanding the meridional movement of a ring, although it is difficult to estimate the value. As for the experiments with a different slope, it is obvious that the steeper the slope is, the less the average distance becomes, regardless of whether the rings move westward or not. The effect of bottom friction preventing the northward movement is also in accord with the above discussion, because bottom friction tends to advect a ring offshore through a cyclone generated to the north.

4.3. Applications

In the case of a steep slope, warm-core rings which have deep baroclinic flow move northward (case A in Figure 4). This behavior of warm-core rings is similar to the long-term northward alongshore movement of Kuroshio warm-core rings east of Japan. However, if we compare the model and the real ocean in detail, a few differences appear. Kuroshio warm-core rings move approximately along the 4000-m isobath, but the model rings reach the 2000-m isobath. Furthermore, though Kuroshio warm-core rings sometimes exist for a numbers of years, the model rings must not. After the 200-day calculation the maximum velocity of the model rings decayed to 0.2 m s^{-1} from an initial maximum velocity of 1.1 m s^{-1} (Figure 4). These discrepancies are due to not including the possible effects caused by the presence of other warm-core rings and the Oyashio in our model. Kuroshio warm-core rings were often observed interacting with newly generated warm-core rings from the south and with offshore warm-core rings from the east [Tomosada, 1986; Yasuda *et al.*, 1992; Yasuda, 1995]. Merging with offshore rings and mutual advection with southern rings should result in the eastward and northward movement of the warm-core rings, respectively [Yasuda, 1995]. This merging process also supplies these warm-core rings with energy and vorticity [Yasuda, 1995]. The actual interactions are not as simple, but warm-core rings 86B and 93A were observed to move offshore and increase their core temperatures, through interactions with the Kuroshio Extension and offshore rings. The Oyashio front in the Kuroshio-Oyashio transition zone has twig-like paths [Kawai, 1972], and warm-core rings are often surrounded by the intruding Oyashio. The first Oyashio intrusion, the nearest intrusion to the shore, may block the warm-core rings from approaching the shore. Therefore we conclude that the basic mechanism of the northward movement of Kuroshio warm-core rings is the equivalent image effect.

An additional application is to the warm eddies in the Gulf of Mexico, where the western boundary is also approximately meridional. The movement of the eddies in the Gulf of Mexico is, however, very different from the Kuroshio warm-core rings. The eddies in the Gulf of Mexico originate from the Loop Current and move not to the north but to the west, interacting with the bottom topography of the Gulf [Elliott, 1982; Vucovich and Waddell, 1991]. When they reach the western end of the Gulf, the interaction is very destructive and sometimes expressed as "collision." Numerical studies for this region sometimes assumed that the western boundary acted as a vertical wall in the sense that the interaction is a "collision" [Shi and Nof, 1994; Sansón *et al.*, 1998]. This different behavior of the warm eddies in the Gulf of Mexico from Kuroshio warm-core rings is because of the bottom topography of these regions (Figure 11). The slope of the Gulf of Mexico is moderate, and the situation is the same as case F in our experiments. The moderate slope not only causes the weak northward tendency but also permits an eddy to get closer to a coast. The interaction near a coast is destructive, because the upper parts of an eddy interact with bottom topography.

5. Summary

We study the effects of the bottom slope of a western boundary on warm-core rings with a primitive equation sigma coordinate model. The results are summarized as follows.

1. Warm-core rings which initially have baroclinic velocity

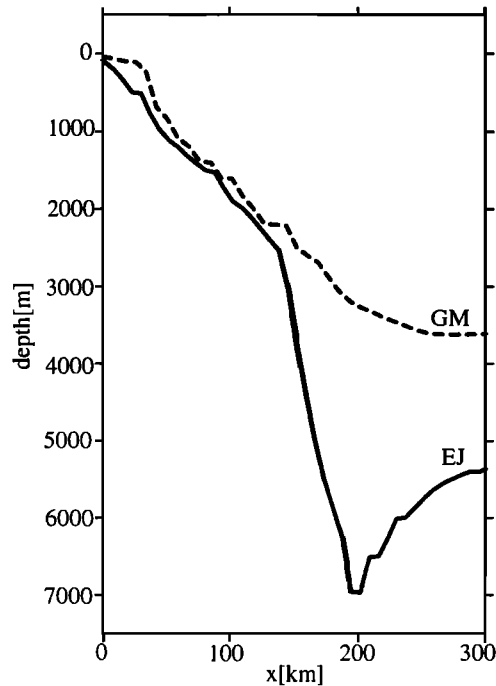


Figure 11. Cross section of the bottom topography east of Japan (EJ: solid line) and the Gulf of Mexico (GM: dashed line), along 39°N and 24°N, respectively. Bottom topography from the coast to 300 km offshore is presented.

near a steep bottom slope move northward. The mechanism of the northward movement is due to an effect equivalent to the image effect, and this effect is the basic mechanism of the long-term northward movement of the Kuroshio warm-core rings.

2. On the contrary, rings which initially have deep barotropic velocity or no velocity at all move southwestward owing to the nonlinear planetary β effect. Barotropic velocity on a steep slope immediately disperses as a topographic Rossby wave, and the ring becomes isostatic.

3. The steeper a slope is, the more the equivalent image effect affects rings through the closer location to a coast. Ring-slope interactions are moderate compared to ring-wall interactions because they take place at a depth where the velocity of rings is relatively weak.

4. Bottom friction decreases the northward movement of rings through the eastward advection of cyclonic eddies generated at the north of rings. As in the consideration of the gradient of a slope, the effect of cyclonic eddies in the case with a slope is weaker than that of a no-slip wall.

Our model creates a very simple understanding of the topographic effects, but realistic phenomena are reproduced as well. For future research we plan to investigate the effects of different boundary orientations, since this seems to be an important factor in the behavior of warm-core rings.

References

Ball, F. K., Some general theorems concerning the finite motion of a shallow rotating liquid lying on a paraboloid, *J. Fluid Mech.*, 17, 240–256, 1963.
 Brown, O. B., P. C. Cornillon, S. R. Emmerson, and M. H. Carle, Gulf Stream warm rings: A statistical study of their behavior, *Deep Sea Res., Part 1*, 33, 1459–1473, 1986.

Cox, M. D., A numerical study of Somali Current Eddies, *J. Phys. Oceanogr.*, 9, 311–326, 1979.
 Cushman-Roisin, B., E. P. Chassignet, and B. Tang, Westward motion of mesoscale eddies, *J. Phys. Oceanogr.*, 20, 758–768, 1990.
 Elliott, B. A., Anticyclonic rings in the Gulf of Mexico, *J. Phys. Oceanogr.*, 12, 1292–1309, 1982.
 Hata, K., Behavior of a warm eddy detached from the Kuroshio (in Japanese, English abstract), *J. Meteorol. Res.*, 26, 295–321, 1974.
 Hogg, N. G., and H. M. Stommel, The Heton: An elementary interaction between discrete baroclinic geostrophic vortices and its implications concerning eddy-head flow, *Proc. R. Soc. London, Ser. A*, 397, 1–20, 1985.
 Hoskins, B. J., M. E. McIntyre, and A. W. Robertson, On the use and significance of isentropic potential vorticity maps, *Quart. J. R. Meteorol. Soc.*, 111, 877–946, 1985.
 Itoh, S., On the mechanism of the movement of warm-core rings off Sanriku (in Japanese), master thesis, 81 pp., Univ. of Tokyo, March 1999.
 Kawai, H., Hydrography of the Kuroshio Extension, in *The Kuroshio*, edited by H. Stommel and K. Yoshida, pp. 235–352, Univ. of Tokyo Press., 1972.
 Kawasaki, Y., T. Kono, and T. Sugimoto, Velocity fluctuation in the Oyashio (in Japanese), *Mar. Monthly*, 22, 199–210, 1990.
 Killworth, P. D., On the motion of isolated lenses on a beta-plane, *J. Phys. Oceanogr.*, 13, 368–376, 1983.
 Kitano, K., Some properties of the warm eddies generated in the Confluence Zone of the Kuroshio and Oyashio Currents, *J. Phys. Oceanogr.*, 5, 245–252, 1975.
 Matsuura, T., and M. Kamachi, The behavior of Kuroshio warm-core rings near the eastern coast of Japan, in *Mesoscale/Synoptic Coherent Structures in Geophysical Turbulence*, edited by J. C. J. Nihoul and B. M. Jamart, pp. 562–576, Elsevier Sci., New York, 1989.
 McWilliams, J. C., and G. R. Flierl, On the evolution of isolated, nonlinear vortices, *J. Phys. Oceanogr.*, 9, 1155–1182, 1979.
 Mellor, G. L., User's guide for a three-dimensional, primitive equation, numerical ocean model, 41 pp., Program in Atmos. and Oceanic Sci., Princeton Univ., Princeton, N.J., 1998.
 Mellor, G. L., T. Ezer, and L.-Y. Oey, The pressure gradient conundrum of sigma coordinate ocean models, *J. Atmos. Oceanic Technol.*, 11, 1126–1134, 1994.
 Mertz, G., and D. Wright, Interpretations of the JEBAR term, *J. Phys. Oceanogr.*, 22, 301–305, 1992.
 Nof, D., On the β -induced movement of isolated baroclinic eddies, *J. Phys. Oceanogr.*, 11, 1662–1672, 1981.
 Nof, D., Strange encounters of eddies with walls, *J. Mar. Res.*, 57, 739–761, 1999.
 Sansón, L. Z., and G. J. F. van Heijst, Interaction of barotropic vortices with coastal topography: Laboratory experiments and numerical simulations, *J. Phys. Oceanogr.*, 30, 2141–2162, 2000.
 Sansón, L. Z., F. Graef, and E. G. Pavia, Collision of anticyclonic, lense-like eddies with a meridional western boundary, *J. Geophys. Res.*, 103, 24,881–24,890, 1998.
 Sansón, L. Z., G. J. F. van Heijst, and F. J. J. Janssen, Experiments on barotropic vortex-wall interaction on a topographic β plane, *J. Geophys. Res.*, 104, 10,917–10,932, 1999.
 Shi, C., and D. Nof, The destruction of lenses and generation of wadons, *J. Phys. Oceanogr.*, 24, 1120–1136, 1994.
 Smith, D. C., IV, A numerical study of Loop Current Eddy interaction with topography in the western Gulf of Mexico, *J. Phys. Oceanogr.*, 18, 1260–1272, 1986.
 Smith, D. C., IV, and J. J. O'Brien, The interaction of a two-layer isolated mesoscale eddy with bottom topography, *J. Phys. Oceanogr.*, 13, 1681–1697, 1983.
 Sommerfeld, A., *Mechanics of Deformable Bodies*, translated from German by G. Kuerti, 396 pp., Academic, San Diego, Calif., 1950.
 Thierry, V., and Y. Morel, Influence of a strong bottom slope on the evolution of a surface-intensified vortex, *J. Phys. Oceanogr.*, 29, 911–923, 1999.
 Tomosada, A., Generation and decay of Kuroshio warm-core rings, *Deep Sea Res., Part 1*, 33, 1475–1486, 1986.
 Vucovich, F. M., and E. Waddell, Interaction of a warm ring with the western slope in the Gulf of Mexico, *J. Phys. Oceanogr.*, 21, 1062–1074, 1991.
 Yasuda, I., Geostrophic vortex merger and streamer development in

- the ocean with special reference to the merger of Kuroshio warm core rings, *J. Phys. Oceanogr.*, 25, 980–996, 1995.
- Yasuda, I., K. Okuda, and K. Mizuno, Numerical study on the vortices near boundaries: Considerations on warm-core rings in the vicinity of east coast of Japan (in Japanese, English abstract), *Bull. Tohoku Reg. Fish. Res. Lab.*, 48, 67–86, 1986.
- Yasuda, I., K. Okuda, and M. Hirai, Evolution of a Kuroshio warm-core ring: Variability of the hydrographic structure, *Deep Sea Res., Part I*, 39, S131–S161, 1992.
-
- S. Itoh and T. Sugimoto, Division of Fisheries Environmental Oceanography, Ocean Research Institute, University of Tokyo, 1-15-1, Minamidai, Nakano-ku, 164-8639, Japan. (itohsach@ori.u-tokyo.ac.jp; sugimoto@ori.u-tokyo.ac.jp)

(Received January 8, 2001; revised June 7, 2001; accepted July 5, 2001.)